

New concept for VFTO attenuation in GIS with modified disconnecter contact system

Marcin Szewczyk, *Senior Member, IEEE*, Wojciech Piasecki, *Member, IEEE*,
Marcin Wroński, Kamil Kutorasiński

Abstract—This paper investigates on a new concept for Very Fast Transient Overvoltages (VFTO) attenuation in Gas-Insulated Switchgear (GIS). The concept, first introduced by the authors in this paper, involves modification of the GIS disconnecter contact system in order to dissipate the VFTO energy in damping elements placed inside the GIS busbar conductor. The concept is an alternative to the state-of-the-art method in which magnetic rings are placed in the space between the GIS conductor and the enclosure. The proposed arrangement has no impact of the damping element on the dielectric design of the GIS busbar, as well as highly reduces the impact on the GIS thermal design. The paper presents analyses which show feasibility of the concept, through 1) principles which govern voltage conditions inside the GIS busbar, and 2) full-Maxwell FEM electromagnetic simulations of VFTO attenuated with the use of the proposed concept.

Index Terms--Very Fast Transient Overvoltages (VFTO), Gas-Insulated Switchgear (GIS), disconnecter switch, resistive and magnetic material, attenuation, damping, transients, switching

I. INTRODUCTION

Very Fast Transient Overvoltages (VFTO) are generated in Gas-Insulated Switchgear (GIS) mainly due to disconnecter operations, during which pre- and re-strike breakdown flashovers occur in the disconnecter contact system [1-4]. The generated VFTO values are determined by: 1) SF6 gas conditions according to the Toepler equation [5] and 2) initial voltage conditions before the breakdown. The VFTO values are reported as up to 1.5-2.8 p.u. [6], depending on the nominal voltage level of the switchgear and the disconnecter design.

A. Impact of VFTO on GIS substation design

The dielectric design and insulation coordination of the GIS is determined by rated Lightning Impulse Withstand Voltage (LIWV) [6]. Since High Voltage (HV) and Ultra High Voltage (UHV) GIS are designed with a relatively low ratio between LIWV and rated voltage, the VFTO is one of the design factors, specifically important for voltage levels from 800 kV up to 1200 kV [6]. For HV GIS, with rated voltages below and

equal to 550 kV, LIWV is most often not exceeded by VFTO, but the VFTO still affects insulation systems of power equipment, such as transformers [7], bushings [8], and secondary equipment [9], due to the voltage rate of rise (dU/dt) highly exceeding that for a standard LIWV test.

B. Overview of main VFTO attenuation methods

Several methods for VFTO attenuation are currently being investigated. The most up-to-date overview of main methods for VFTO attenuation in GIS is given in papers [10], [11]. They include: disconnecter equipped with damping resistor [12], disconnecter with reduced voltage due to the trapped charge reduction during the disconnecter opening operation (the so called Trapped Charge Voltage, TCV) [3,13], application of high frequency resonators [14], and application of magnetic material of different types [15], [16], [17], [18], [19], [21].

Since of the mentioned above that using the damping resistor and that based on application of magnetic materials are relevant to the new method described in the present paper, they are hence outlined in the following subsections.

C. VFTO attenuation with damping resistor

Disconnecter with a damping resistor is a proven technology [12]. The operation of the disconnecter with damping resistor involves two stages. In the first stage, the spark is flushed between the disconnecter moving contact and the additional resistor. The resistor is connected in series to the fixed contact. The spark energy is dissipated in the resistance of the spark and of the additional resistor. In the second stage, the moving contact is galvanically connected to the fixed contact, thus for the steady state condition, after the disconnecter closing operation is completed, the resistor is eliminated from the circuit. The method is proven to be highly efficient, as it provides almost complete VFTO attenuation [6], [12]. However, the associated disadvantages are significant and include: high energy dissipation requirements for the resistor, special dielectric design requirements for the electric field screening elements around the resistor, flashover risk across the resistor, increase of the disconnecter complexity (reliability and maintenance requirements), special testing requirements (high cost and demanding logistics).

D. VFTO attenuation with magnetic material

Using a magnetic material for attenuation of transients in power system is an interesting damping method, already implemented in practice in MV applications [20]. For HV/UHV GIS, the technology is still in its development stage,

M. Szewczyk, W. Piasecki are with ABB Corporate Research Center, 31-038 Krakow, Starowislna 13A, Poland (e-mail: marcin.szewczyk@pl.abb.com, wojciech.piasecki@pl.abb.com).

M. Wronski and K. Kutorasinski are with AGH University of Science and Technology, Faculty of Physics and Applied Computer Science, 30-059 Kraków, Mickiewicza 30, Poland (email: kamil.kutorasinski@fis.agh.edu.pl, marcin.wronski@fis.agh.edu.pl).

Corresponding author: M. Szewczyk (e-mail: marcin.szewczyk@pl.abb.com).

being discussed as a promising alternative as compared to the solution of the disconnector with damping resistor.

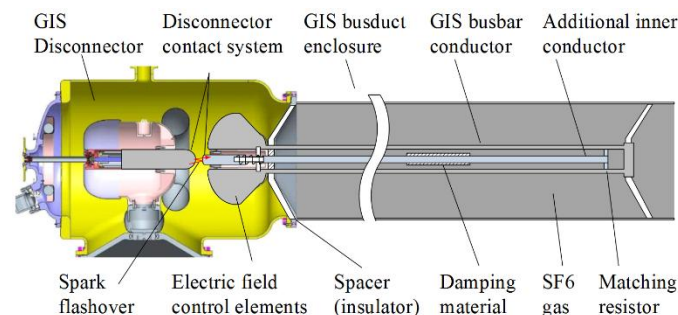


Fig. 1 Concept illustration in exemplary GIS arrangement: GIS disconnector and GIS busduct with additional inner conductor

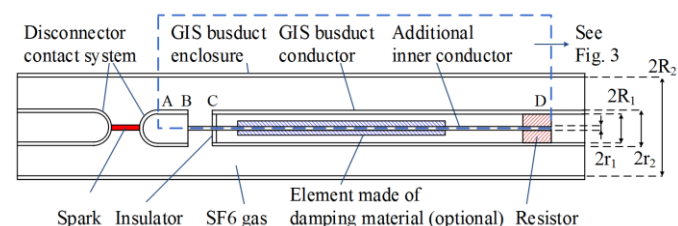


Fig. 2. Simplified GIS geometry assumed for the concept analyses; dashed box area and ABCD points are presented in detail in Fig. 3; R_2 – inner radius of GIS enclosure, r_2 – outer radius of GIS conductor, R_1 – inner radius of GIS conductor, r_1 – outer radius of additional inner conductor

In the magnetic material the energy of the electromagnetic wave propagating through the GIS busduct is dissipated due to the eddy currents and the magnetic hysteresis losses. Different types of magnetic materials are currently under investigation for application in GIS. In [16], [17] the magnetic rings of ferrite type are used in low- and medium- voltage measurement set-up, with the source voltage amplitude value of 0.4 kV in [16] and 3.3 kV in [17]. Measurement results in high voltage set-up are presented in [19] and [21]. In [19] the ferrite rings are used, while in [21] the rings of ferrite and amorphous types are applied.

In each previously referenced papers, when the magnetic rings are of concern [15], [16], [17], [18], [19], [21], the rings are located in the space *between* the GIS busbar conductor and the GIS busbar enclosure. In such case, the dielectric and thermal conditions of the GIS busbar are affected by the rings during the GIS normal operation, which has to be taken into account at the design stage of the equipment.

In this paper, an alternative concept is presented allowing for dissipation of VFTO energy in a magnetic and/or resistive material, with the material being installed *inside* the GIS conductor. The concept involves modification of the disconnector contact system, so that the electromagnetic wave is partially transferred to inside of the GIS conductor. This arrangement eliminates the aforementioned drawbacks associated with the material being installed in the outer space between the GIS conductor and enclosure, namely, eliminating the impact of the magnetic material on electric design and reducing the impact on thermal design of the GIS busbar. The potential advantages of the new concept as compared to the disconnector with damping resistor are also related with that

the damping element(s) are located inside the GIS conductor. Therefore, the space limitations are less severe and in consequence the energy can be dissipated within larger volume available. Moreover, the portion of the dissipated energy can be adjusted by means of the voltage divider ratio and/or transmission/reflection coefficients.

The paper is organized as follows: Section I gives the motivation for Very Fast Transient Overvoltages (VFTO) attenuation in Gas-Insulated Switchgear (GIS) together with the overview of the known attenuation methods, which are most relevant to the new concept introduced in this paper. Section II introduces description of the new concept, together with its exemplary application in the GIS disconnector and GIS busbar arrangement. Section III includes analysis of the concept principles, both analytically and with Finite Element Method (FEM) simulations. Goal of this section is to give understanding of the voltage conditions inside the GIS busbar for when an electromagnetic wave propagates along the busbar. Section IV provides the concept feasibility analysis with full-Maxwell FEM simulations in exemplary VFTO conditions. Section V offers conclusions. Additional conclusions are also included in Sections III and IV (see III.F and IV.D respectively).

II. CONCEPT DESCRIPTION: VFTO ATTENUATION BASED ON RESISTIVE AND MAGNETIC MATERIAL PLACED INSIDE GIS BUSBAR

Fig. 1 illustrates the new damping concept proposed. In the new approach there is an *additional inner conductor* located inside the busbar conductor. The additional inner conductor is located coaxially with respect to the GIS busbar conductor, and it is closed by the element which provides impedance match at the end of the line (matching resistor, see Fig. 1).

Similarly to the aforementioned disconnector equipped with damping resistor (as per [12]), in the concept here proposed the disconnector operation involves three stages.

Stage 1: In the first stage, the spark is flushed between the disconnector moving contact (to which the mechanical propulsion system is linked) and the fixed contact. The fixed contact is modified so that in the opened state its moving element is pulled toward the moving contact so that it attracts the spark flashover from the moving contact. In the closed state, the fixed contact is pulled inside the electric field control elements. In that way, the spark flashover occurs between the moving contact and the fixed contact. The fixed contact is connected to the additional inner conductor through an insulator spacer, in a way which allows the electromagnetic energy to propagate inside the GIS busbar conductor. The spark energy is propagating in a form of the electromagnetic wave inside the GIS conductor. This energy is dissipated inside the conductor, in the matching resistor in the end of the line and/or in the magnetic material located inside the conductor (between the disconnector and the matching element).

Stage 2: In the second stage, the moving contact is galvanically connected to the fixed contact.

Stage 3: In the third stage, both the moving contact and the

fixed contact are connected to the GIS busbar conductor, so that for the steady state condition, after the disconnecter closing operation is completed, the additional inner conductor is eliminated from electric circuit.

In the new concept the electromagnetic wave constituting the VFTO propagates partially inside the GIS busbar conductor. The voltage divider ratio (see explanation further in the article) defines and the part of electromagnetic wave which is propagating between the GIS busbar conductor and the additional inner conductor. This wave is terminated at the end of the GIS busbar conductor by an element providing impedance match which causes that the travelling wave is not reflected and its energy is dissipated. The impedance matching element can be a lumped matching resistor or distributed arrangements known in high frequency applications and used for eliminating reflections in waveguides (e.g. cone arrangement, as in [22]). The energy dissipated in the matching element can be adjusted by means of the voltage divider ratio, which in turn can be adjusted by the diameter of the additional inner conductor. The voltage conditions are also governed by transmission and reflection coefficients at the point of the surge impedance discontinuity, so that the fraction of the VFTO energy can be also controlled by the transmission/reflection conditions, which in turn can be controlled either by dimensioning of the additional inner conductor or by selecting the desired value of the resistor. The

matching element should be dimensioned according to the expected maximum value of the energy dissipated. In order to facilitate a better attenuation of the energy of the travelling wave between the disconnecter and the matching element, additional elements which can absorb the travelling wave energy, such as magnetic material cores (rings) may be located inside the GIS conductor. This could further reduce requirements for the matching element, minimizing the energy at the end of the line, when the energy is partially dissipated due to the eddy currents and the magnetic hysteresis losses in the magnetic material cores. The more optimized magnetic material (i.e. the material type and dimensions), the more energy is dissipated before the travelling wave reaches the resistor. The advantages of using the magnetic material inside the GIS busbar conductor, as opposed to when the material is installed between the GIS busbar conductor and enclosure, is that there is no need for any additional screening elements around the magnetic material. Therefore there is no impact of the material on the dielectric and thermal design of the GIS busbar.

Next sections provide the concept through analysis from the perspective of voltage conditions inside the GIS busbar: Section III presents principles, Section IV provides concept feasibility in VFTO conditions. Additional remarks are included in the conclusion section: Section V.

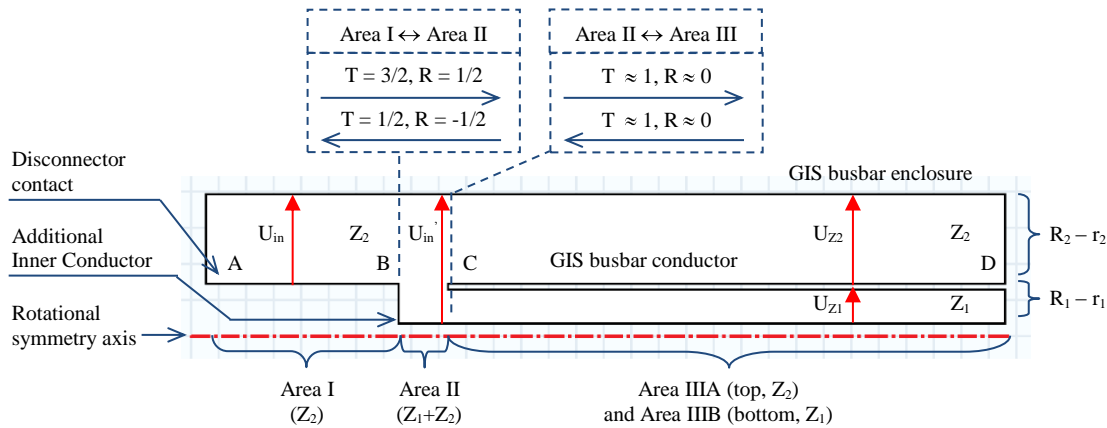


Fig. 3. Axially symmetrical geometry assumed for the concept analyses and FEM simulations (ABCD as per Fig. 2); symbols used: T, R – transmission and reflection coefficients respectively, Z_1 , Z_2 – surge impedances in different areas, U_{in} , U'_{in} , U_{Z1} , U_{Z2} – voltages in Area I, Area II, Area III, $(R_2 - r_2)$ – distance between GIS enclosure and GIS conductor, $(R_1 - r_1)$ – distance between GIS conductor and additional inner conductor; analyses presented in Section III

III. VOLTAGE CONDITIONS: CAPACITIVE VOLTAGE DIVIDER WITH TRANSMISSION AND REFLECTION COEFFICIENTS

A. Model description

For the purpose of presenting the concept principles, a simplified GIS geometry was assumed, as shown in Fig. 2, consisting of main elements of the general concept arrangement. The following elements are included in Fig. 2: 1) the simplified disconnecter contact system, 2) the arrangement of the three coaxial lines: GIS conductor, GIS enclosure, the additional inner conductor, 3) the arrangement of the matching element (resistor) and the magnetic material.

In order to present the concept principles, voltage conditions were analyzed and FEM simulations were conducted, for the selected areas of the GIS busbar, as indicated in Fig. 2 and shown in Fig. 3.

The voltage conditions resulting from the spark ignition in the disconnecter contact system are governed by the voltage divider principle formed by surge impedances of the GIS busduct, and by the transmission and reflection coefficients at the points of the surge impedance discontinuities.

For analyzing the voltage conditions in the GIS busbar, FEM simulations were conducted for the geometry shown in Fig. 3. The geometry in Fig. 3 is a part of the geometry shown in Fig. 2, as indicated in Fig. 2 with a dashed box. For FEM

simulations COMSOL RF solver was used [23].

In the FEM simulations, the input voltage, corresponding to the initial voltage after the spark ignition, was assumed as 1 V. The electromagnetic wave propagating as a result of the initial input voltage, caused a time-variant electromagnetic field distribution along the GIS busduct. For the analyses, the following three areas of the GIS busbar were selected (see Fig. 3): Area I (input voltage U_{in} , corresponding to the initial voltage after the spark ignition), Area IIIA (voltage U_{Z2} between the GIS conductor and the GIS enclosure), Area IIIB (voltage U_{Z1} between the GIS conductor and the additional inner conductor).

As mentioned before the voltage conditions in the GIS busbar (see Fig. 3) are governed by the principle of voltage divider and the principle of electromagnetic wave transmissions and reflections at the points of the surge impedance discontinuity between Areas I/II/III with the corresponding transmission T and reflection R coefficients. The voltage divider is formed by the three coaxial lines: GIS enclosure, GIS conductor, and additional inner conductor, with the input voltage denoted as U_{in}' , and the output voltage as U_{Z1} .

The two principles are addressed in the following subsections, followed by the FEM simulation results of the three voltages: U_{in} , U_{Z1} , and U_{Z2} .

B. Radius of additional inner conductor

The radius of the additional inner conductor defines the surge impedance Z_I associated with the two coaxial lines: the GIS conductor and the additional inner conductor; therefore it affects the voltage U_{Z1} which across the interior of the GIS conductor (being a fraction of the input voltage U_{in}'). The conductor radius also affects the electric field gradient inside the GIS conductor (in the space between the additional inner conductor and the GIS conductor). This electric field can cause a risk of the flashover inside the GIS conductor, which should be avoided by a proper dimensioning of the additional inner conductor.

For the above reasons, it is assumed, that case-by-case dimensioning of the additional inner conductor can be based on a proper selection of the two surge impedances (see Fig. 3): Z_I – surge impedance formed with GIS conductor and additional inner conductor; Z_2 – surge impedance formed with GIS conductor and GIS enclosure.

Assuming that:

$$Z_1 = n Z_2, \quad (1)$$

where n is a multiplying factor here defined, the outer radius r_1 of the additional inner conductor can be expressed as:

$$\ln \frac{R_1}{r_1} = n \cdot \ln \frac{R_2}{r_2} \Rightarrow r_1 = \frac{R_1}{\frac{R_2}{r_2}^n} \quad (2)$$

where (see Fig. 2): R_2 is the inner radius of GIS enclosure, r_2 is the outer radius of GIS conductor, R_1 is the inner radius of

GIS conductor. The radiuses R_2 , r_2 , R_1 are assumed constant, as for the specific GIS design.

C. Voltage divider

In the geometry shown in Fig. 3, the voltage divider is formed by the three coaxial lines: GIS conductor, GIS enclosure, and the additional inner conductor. The input voltage of the divider is denoted as U_{in}' , and the output voltage is denoted as U_{Z1} (the latter is the voltage between the GIS conductor and the additional inner conductor). For the surge impedances Z_1 and Z_2 , as introduced in (1), the output voltage U_{Z1} can be expressed according to the voltage divider formula (for $n = 2$):

$$U_{Z1} = \frac{1}{1 + \frac{Z_2}{nZ_1}} U_{in}' = \frac{1}{1 + \frac{1}{n}} U_{in}' = \frac{2}{3} U_{in}' \quad (3)$$

where n is defined in (1), and Z_1 , Z_2 , U_{Z1} , U_{Z2} , U_{in}' are defined in Fig. 3. It is seen that for higher n value, the radius r_1 significantly decreases, and thus the voltage divider ratio U_{Z1}/U_{in}' increases. This means that for higher n , higher portion U_{Z1} of the input voltage U_{in}' enters to the space between the GIS conductor and the additional inner conductor.

D. Transmission and reflection coefficients

The voltage waves which enter the coaxial lines arrangement, are governed by the electromagnetic wave transmission and reflection laws at the points of the coaxial line surge impedance discontinuity.

The corresponding transmission T_{12} and reflection R_{12} coefficients for the waves propagating from line 1 to line 2, are given by the well-known formulas [25]:

$$T_{12} = \frac{2Z_{02}}{Z_{02} + Z_{01}}, \quad R_{12} = \frac{Z_{02} - Z_{01}}{Z_{02} + Z_{01}}, \quad T = R + 1 \quad (4)$$

where: Z_{02} and Z_{01} are the surge impedances of the lines: to which (Z_{02}), and from which (Z_{01}) the electromagnetic wave propagates. Index 0 in the formulas (4) is used for distinguishing the general relations shown in (4) from the relations shown further in this section in (5) and (6), as obtained for specific geometry in Fig. 3.

For geometry shown in Fig. 3, the following four areas are distinguished, having different surge impedances: Area I (with surge impedance Z_I), Area II (with surge impedance Z_I+Z_2), Area IIIA (with surge impedance Z_2), and Area IIIB (with surge impedance Z_I). The following notation is here introduced and used further in this section: index $I \rightarrow II$ denotes transmission or reflection coefficient from Area I to Area II, and index $I \leftarrow II$ denotes transmission or reflection coefficient from Area II to Area I (e.g. $T_{I \rightarrow II}$ or $R_{I \leftarrow II}$).

It should be noted, that the only significant surge impedance discontinuity in the geometry in Fig. 3 is between Area I (with surge impedance Z_2) and Area II (with surge impedance Z_I+Z_2). Assuming that the GIS conductor thickness is much lower than the GIS busduct dimension ($r_2 - R_1 \ll R_2$), the reflection between Area II and Area III

can be neglected, and thus: $T_{II \rightarrow III} = 1$, $R_{II \rightarrow III} = 0$.

The transmission $T_{I \leftrightarrow II}$ and reflection $R_{I \leftrightarrow II}$ coefficients between Area I (Z_2) and Area II ($Z_1 + Z_2$) are calculated below in (5) and (6) for $n = 2$ (i.e. $Z_1 + Z_2 = 3Z_2$), where: index I \rightarrow II denotes transmission and reflection coefficients from Area I (Z_2) to Area II ($2Z_2 + Z_2 = 3Z_2$), and index II \rightarrow I denotes transmission and reflection coefficients from Area II ($3Z_2$) to Area I (Z_2).

Table I provides summary of the calculated transmission and reflection coefficients. It can be easily noted that the relation $T = R + 1$ is fulfilled. The calculated values are also indicated in Fig. 3.

$$T_{12} = \frac{2Z_{02}}{Z_{02} + Z_{01}} \rightarrow \begin{aligned} T_{I \rightarrow II} &= \frac{2 \cdot 3Z_2}{3Z_2 + Z_2} = +\frac{3}{2} \\ T_{I \leftarrow II} &= \frac{2 \cdot Z_2}{3Z_2 + Z_2} = +\frac{1}{2} \end{aligned} \quad (5)$$

$$R_{12} = \frac{Z_{02} - Z_{01}}{Z_{02} + Z_{01}} \rightarrow \begin{aligned} R_{I \rightarrow II} &= \frac{3Z_2 - Z_2}{3Z_2 + Z_2} = +\frac{1}{2} \\ R_{I \leftarrow II} &= \frac{Z_2 - 3Z_2}{3Z_2 + Z_2} = -\frac{1}{2} \end{aligned} \quad (6)$$

TABLE I
Transmission T and reflection R coefficients,
n – multiplying factor defined in (1)

	Transmission T [-]	Reflection R [-]
Area: I \rightarrow II	3/2 (for $n = 2$)	1/2 (for $n = 2$)
Area: I \leftarrow II	1/2 (for $n = 2$)	-1/2 (for $n = 2$)
Area: II \rightarrow III	~ 1	~ 0
Area: II \leftarrow III		

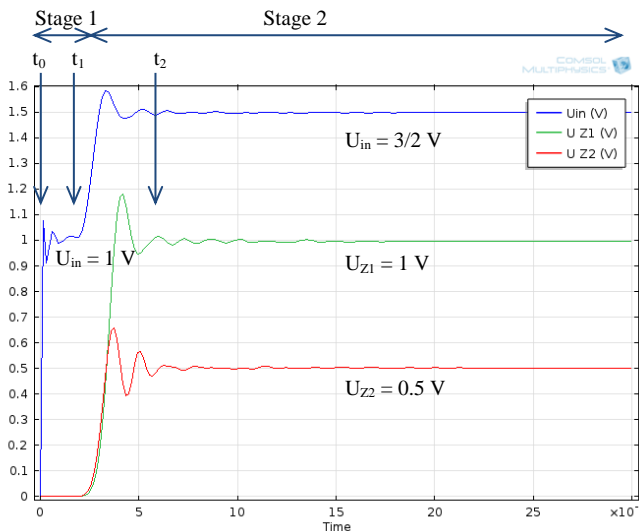


Fig. 4. Voltages U_{in} (top), U_{Z1} (middle), U_{Z2} (bottom), as indicated in Fig. 3, as a function of time; in steady state condition ($t = 30$ ns) reflecting the electric field distribution shown in Fig. 5 ($U_{in} = 3/2$ V, $U_{Z1} = 1$ V, $U_{Z2} = 0.5$ V); for Case 1 ($R = Z_1$; matched)

E. FEM simulation results

In order to analyze voltage conditions in the GIS busbar in Fig. 3, two simulation cases were conducted: Case 1 (with

matching resistor $R = Z_1$; matched), and Case 2 (with matching resistor $R = 0$; earthed). Electromagnetic wave was generated at the input port of geometry (U_{in} in Fig. 3). Then the transient response to a step function was simulated.

The simulations were performed for the geometrical dimensions of the additional inner conductor corresponding to the multiplying factor $n = 2$, as defined in (1). Thus, the voltage divider condition is given by (3) and the transmission and reflection coefficients are given by (5) and (6) respectively. The analysis of the FEM simulation results are conducted based on (3), (5), (6).

Case 1 ($R = Z_1$; matched). In Fig. 4 the time functions of the three voltages are shown: U_{in} , U_{Z1} , U_{Z2} , as indicated in Fig. 3.

In Fig. 5 the electric field distribution is shown for the steady state condition, at the time instance $t = 30$ ns after the spark ignition. In the steady state condition, the voltages have the following values: $U_{in} = 3/2$ V, $U_{Z1} = 1$ V, and $U_{Z2} = 0.5$ V, which is visible both in Fig. 4 and in Fig. 5.

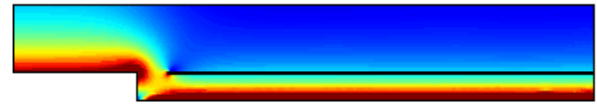


Fig. 5. Distribution of electric field norm in steady state condition ($t = 30$ ns) inside the GIS busbar according to Fig. 3; for Case 1 ($R = Z_1$; matched)

The following is the discussion of the voltage functions in Fig. 4. In the initial stage, the input voltage U_{in} increases from 1 V to $3/2$ V in the steady state. This is due to the reflection from the surge impedance discontinuity between Area I and Area II (see Fig. 4 and also description below). In the steady state condition, the set-up behaves as a voltage divider according to (3) with the following voltage split (for $n = 2$):

$$U_{Z1} = \frac{1}{1 + \frac{1}{2}} U'_{in} = \frac{2}{3} U'_{in}; \quad U_{Z2} = U'_{in} - U_{Z1} = \frac{1}{3} U'_{in}$$

where U'_{in} is given by the initial voltage of 1 V multiplied by transmission factor (3/2), thus $U_{in} = 3/2$ V (see Fig. 4).

The time sequence of the travelling waves is as follows (see Fig. 4 for time instances denoted as t_0 , t_1 , and t_2): t_0 – Simulation starts, the travelling wave is initiated at the input of the geometry in Fig. 3 (left hand side), and it reaches point of U_{in} measurement (as indicated in Fig. 3), with the value of 1 V; t_1 – The wave reaches the U_{in} measurement point after being reflected at the discontinuity between Area I and Area II with reflection coefficient of $+1/2$ (see Fig. 3 and Table I), thus the original 1 V becomes $(1 \text{ V} + 1/2 * 1 \text{ V}) = 3/2 \text{ V}$. Moreover, according to the transmission factor $3/2$ between Area I and Area II (see Fig. 3 and Table I), the initial voltage 1 V is transmitted at the discontinuity point as $3/2 * 1 \text{ V} = 3/2 \text{ V}$. According to the voltage divider formula (3) with factor $1/3$ on Z_2 and $2/3$ on Z_1 , the value $3/2$ V is split between Z_2 and Z_1 accordingly: $U_{Z2} = 1/3 * 3/2 \text{ V} = 1/2 \text{ V}$ and $U_{Z1} = 2/3 * 3/2 \text{ V} = 1 \text{ V}$; t_2 – Steady state condition is reached with the aforementioned values: $U_{Z2} = 1/2 \text{ V}$ and $U_{Z1} = 1 \text{ V}$.

The description of the voltage conditions in the GIS busduct presented above gets significantly complicated for the Case 2 (with $R = 0$; earthed). For this reason, the diagrams were introduced in Fig. 6 in order to present the travelling waves sequence together with the amplitudes associated to the waves in specific time instances. In Fig. 6 the diagrams are presented for Case 1 ($R = Z_1$; matched), according to the travelling waves description provided above. The diagrams reflect simulation results shown in Fig. 4. The two stages in Fig. 6 are also indicated in Fig. 4.

Case 2 ($R = 0$, earthed). In Fig. 7 the time functions of the three voltages are shown: U_{in} , U_{Z1} , U_{Z2} , as indicated in Fig. 3.

In Fig. 8a the electric field distribution is shown for the steady state condition, at the time instance $t = 30$ ns after the spark ignition. In the steady state condition, the voltages have the following values: $U_{in} = U_{Z2} = 1$ V, $U_{Z1} = 0$ V, which is visible in both Fig. 7 and in Fig. 8a.

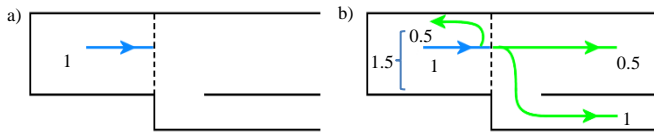


Fig. 6. Voltage diagram for Fig. 4: a) Stage 1 and b) Stage 2

Using the diagrams introduced above for the analysis of Case 1, as well as using the voltage divider conditions in (3) and the transmission and reflection coefficients in (5) and (6) (see also Fig. 3 and Table I), the three stages of the travelling waves conditions as indicated in Fig. 7 are shown in Fig. 6b. In Case 2, stage 1 and stage 2 are the same as for Case 1 (as shown in Fig. 6a and Fig. 6b respectively). Fig. 8b explains voltage conditions in Case 2 Stage 3, as also indicated in Fig. 7.

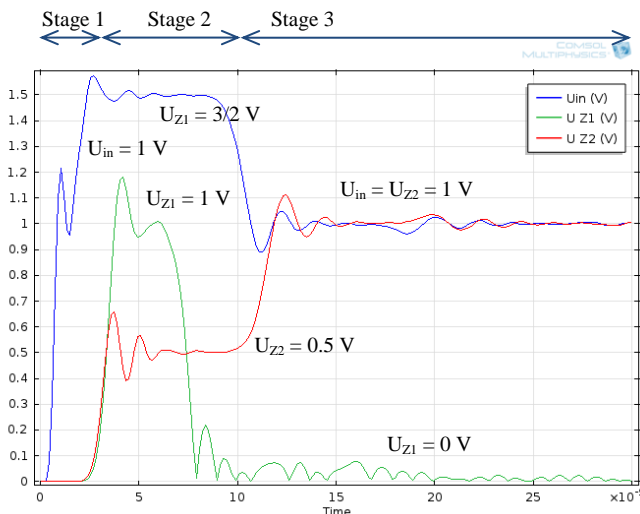


Fig. 7. Voltages U_{in} (top), U_{Z1} (middle), U_{Z2} (bottom), as indicated in Fig. 3, as a function of time; in steady state condition ($t = 30$ ns) reflecting the electric field distribution shown in Fig. 8a ($U_{in} = U_{Z2} = 1$ V, $U_{Z1} = 0$ V); for Case 2 ($R = 0$; earthed)

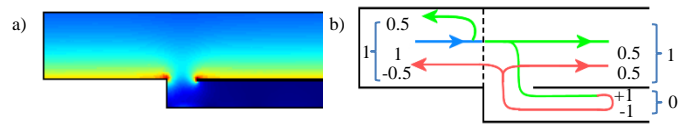


Fig. 8. a) Distribution of electric field norm in steady state condition ($t = 30$ ns) inside the GIS busbar according to Fig. 3, b) Voltage diagram for Fig. 7 – Stage 3; for Case 2 ($R = 0$; earthed)

F. Conclusions from Section III

It has been demonstrated that the set-up analyzed works as a voltage divider. The input voltage value depends on the transmission and reflection coefficients, which are in turn based on the surge impedance values at the points of the surge impedance discontinuity. The voltage conditions due to the travelling wave propagating inside the GIS busbar gets significantly complicated for the cases with travelling wave multiple reflections (see Case 2 above). The diagrams were introduced to present the travelling waves sequence together with the associated amplitudes. Good agreement between analytical analyses and FEM numerical simulations was presented.

IV. ANALYSIS OF CONCEPT FEASIBILITY: FULL-MAXWELL FEM SIMULATIONS IN VFTO CONDITIONS

A. Model description

In order to analyze the technical feasibility of the concept proposed, FEM simulations were conducted for the geometry shown in Fig. 9.

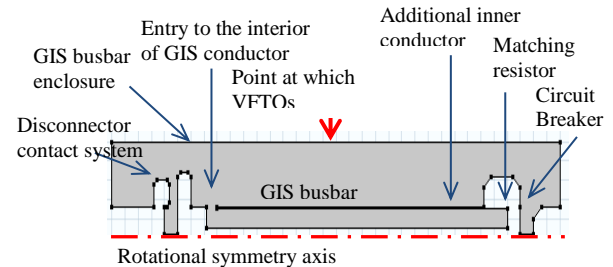


Fig. 9. Simplified GIS geometry for prove of concept through full-Maxwell FEM simulations in exemplary VFTO conditions; VFTO conditions are introduced through the geometry complexity; analyses presented in Section IV

The geometry shown in Fig. 9 reproduces VFTO conditions in a simplified, however realistic GIS arrangement. The simplified models of two switching devices were introduced: disconnector and circuit breaker, together with the GIS busbar located in between the switching devices. The GIS busbar is arranged in a way which allows the travelling wave to enter the interior of the GIS conductor (space between the GIS conductor and the additional inner conductor). In a reference case, when no VFTO attenuation is introduced, the entry is closed by a conductive element (not shown in Fig. 9).

B. Simulation sequence

The simulation sequence employed for the VFTO generation was set-up according to the test procedure for the GIS disconnector type testing, as per IEC Standard [26]. It consisted of two steps. Step 1: In the first step the voltage was

established on the GIS busduct between the opened disconnector and the opened circuit breaker (the so called Trapped Charge Voltage, TCV). This allowed to establish the worst case initial conditions for VFTO generation, which took place in the second step. After the busbar was charged with TCV, it stayed insulated in the course of the rest of the simulation. Step 2: The second step was the main part of the simulation. The breakdown was simulated in the disconnector contact system, causing that the voltage trapped in the GIS busbar (TCV) was released. The VFTO was generated as a result of multiple interferences from points of surge impedance discontinuity. For VFTO to be generated, some degree of the geometry complexity is necessary in order to introduce multiple interferences, which lead to the final VFTO wave shape. The geometry assumed in Fig. 9 allowed to generate an exemplary VFTO waveform with a maximum amplitude of 1.7 p.u. (see Fig. 10).

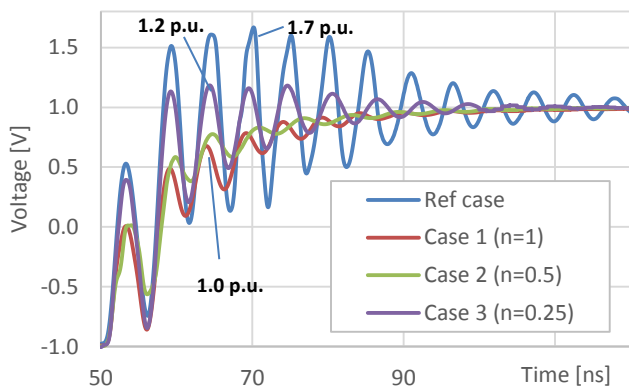


Fig. 10. VFTO waveforms simulated for geometry in Fig. 9: a) reference case (no VFTO attenuation), simulation cases according to Table II ($n = 1.00, 0.50, 0.25$)

C. FEM simulation results

Simulations were conducted for four cases, characterized by different values of the multiplying factor n , as defined in (1). Thus, for each case, different radius r_1 or the additional inner conductor was used, which in turn caused different voltage fractions entering to the GIS conductor (i.e. to the space between the GIS conductor and the additional inner conductor).

Table II provides summary of the conducted simulation cases (radius r_1 is expressed in p.u., where 1 p.u. is for the case with $n = 1$, and VFTO is expressed in p.u., where 1 p.u. equals to the rated voltage multiplied by $\sqrt{2/3}$). Voltage divider ratio U_{Z1}/U'_{in} is included in Table II for the purpose to indicate the general trend of the voltage fraction, being propagated inside the GIS conductor.

TABLE II
Radius r_1 of additional inner conductor for different values of multiplying factor n

Case No	n [-]	r_1 [p.u.]	U_{Z1}/U'_{in} [-]	VFTO [p.u.]
Reference	0.00	-	-	1.7
Case 1	1.00	1.0	0.50	1.2

Case 2	0.50	1.8	0.33	0.0
Case 3	0.25	2.6	0.20	0.0

Since for Case 1 (with $n = 1$), the VFTO attenuation was already very high, the two additional cases were calculated, as characterized with lower n values ($n < 1$): Case 2 with $n = 0.50$ and Case 3 with $n = 0.25$. This allowed to illustrate the level to which the VFTO attenuation is influenced by the additional inner conductor radius r_1 .

Fig. 10 shows simulation results conducted for the geometry in Fig. 9 and for the dimensions of the additional inner conductor specified in Table II. In the reference case, where no VFTO attenuation is introduced, the VFTO reaches 1.7 p.u.

D. Conclusions from Section IV

VFTO attenuation for the new concept was presented for the exemplary VFTO conditions introduced with the use of the model in Fig. 9. Simulation results are shown in Fig. 10. Significant reduction of VFTO is observed. Moreover, lower diameter r_1 of the additional inner conductor (higher n factor) causes, that: a) the distance between the GIS conductor and the additional inner conductor is higher, thus b) the associated surge impedance Z_1 is higher, thus c) the associated voltage U_{Z1} of the voltage divider is higher, thus d) the higher fraction of the input voltage is conducted inside the GIS conductor, thus e) more energy is dissipated in the resistor at the end of the GIS conductor, thus f) the VFTO attenuation is more efficient.

V. CONCLUSIONS

Application of magnetic materials for VFTO attenuation in GIS is gaining an interest among researchers as a promising method for VFTO attenuation (most recently in [21]). The method with magnetic materials is perceived as an alternative solution compared to the disconnector with damping resistor, but it affects the dielectric and thermal design of the GIS busduct. In this paper, a new method on VFTO attenuation is presented, together with its feasibility analyses. The concept introduces an additional inner conductor inside to the GIS conductor, being closed by the element which provides impedance match at the end of the line.

This arrangement have the following features: 1) It is a voltage divider, i.e. only a given part of the VFTO is conducted inside the GIS conductor; 2) At the end of the GIS conductor there is an element providing impedance match (e.g. a resistor), which causes that the travelling wave is not reflected and its energy is dissipated in the matching element. The energy can be adjusted by means of the voltage divider ratio, which in turn can be adjusted by the diameter of the additional inner conductor, or by the transmission/reflection coefficients at the point of impedance discontinuity; 3) The energy can be further dissipated by the eddy currents and the magnetic hysteresis losses in the magnetic material cores (rings) placed inside the GIS conductor. The proposed arrangement requires careful dielectric design of the disconnector contact system to avoid flashovers between the additional inner conductor and the disconnector, or GIS

busbar, elements.

The presented analyses and FEM simulation results illustrate the principles on the concept and show the concept application in a simplified, however realistic GIS geometry in exemplary VFTO conditions.

The proposed concept allows to apply a magnetic material inside the GIS conductor. This arrangement will cause no impact of the magnetic material on the dielectric design and significantly limited impact on the thermal design of the GIS busbar.

VI. REFERENCES

- [1] S.A. Boggs, F.Y. Chu, N. Fujimoto, A. Krenicky, A. Plessl, D. Schlacht "Disconnect Switch Induced Transients and Trapped Charge in Gas-Insulated Substations," *IEEE Trans. PAS-101*, October, 1982.
- [2] N. Fujimoto, H.A. Stuckless, S.A. Boggs, "Calculation of disconnecter induced overvoltages in gas-insulated substations," *Gaseous Dielectrics IV*, L. Christophorou ed. Pergamon Press, 1984.
- [3] S.A. Boggs, N. Fujimoto, M. Collod, E. Thuries "The Modeling of Statistical Operating Parameters and The Computation of Operation-Induced Surge Wave-forms for GIS Disconnectors," 1984 *CIGRE*, paper 13-15.
- [4] J. Meppelink, K. Diederich, K. Feser, W. Pfaff, "Very fast transients in GIS," *IEEE Trans. Power Delivery*, vol. 4, pp. 223-233, Jan. 1989
- [5] D. Povh, H. Schmitt, O. Volcker, R. Witzmann, P. Chewdhuri, A. E. Imece, R. Iravani, J. A. Martinez, A. Keri, A. Sarshar, "Modeling and Analysis Guidelines for Very Fast Transients," *IEEE Power Engineering Review*, vol. 17, Issue 13, 1996
- [6] U. Riechert, C. Neumann, H. Hama, U. Schichler, S. Okabe, "Very Fast Transient Overvoltages (VFTO) in Gas-Insulated UHV Substations," *DI.03 CIGRE Advisory Group Report*
- [7] CIGRE JWG A2-A3-B3.21, "Electrical Environment of Transformers – Impact of Fast Transients", *Electra* No. 218, Feb. 2005, pp. 25-37
- [8] K. Johansson, U. Gäfvert, G. Eriksson, L. Johansson, "Modeling and Measurements of VFT Properties of a Transformer to GIS Bushing", *A2.302.2010, CIGRE 2010*
- [9] CIGRÉ Working Group A3.22: "Background of Technical Specifications for Substation Equipment Exceeding 800 kV AC," *CIGRÉ Brochure No. 456, April 2011*
- [10] A. Tavakoli, A. Gholami, H. Nouri, M. Negnevitsky, "Comparison between suppressing approaches of Very Fast Transients in Gas-Insulated Substations (GIS)," *IEEE Trans. Power Delivery*, vol. 28, pp. 303-310, Jan 2013
- [11] U. Riechert, M. Bösch, M. Szweczyk, W. Piasecki, J. Smajic, A. Shoory, S. Burow, S. Tenbohlen, Mitigation of Very Fast Transient Overvoltages in Gas Insulated UHV Substations, *CIGRE 2012*
- [12] Y. Yamagata, K. Tanaka, S. Nishiwaki, N. Takahashi, T. Kokumai, I. Miwa, T. Komukai, K. Imai, "Suppression of VFT in 1100 kV GIS by adopting resistor-fitted disconnecter," *IEEE Tran. Power Delivery*, vol. 1, pp. 872-880, April 1996
- [13] Szweczyk M., Piasecki W., Stosur M., Riechert U., Kostovic J., "Impact of Disconnector Design on Very Fast Transient Overvoltages in Gas-Insulated UHV Switchgear", *Proceedings of 17th International Symposium on High Voltage Engineering (ISH)*, August 22nd – 26th, Hannover, Germany
- [14] J. Smajic, W. Holaus, A. Troeger, S. Burow, R. Brandl, S. Tenbohlen "HF Resonators for Damping of VFTs in GIS", *International Conference on Power Systems Transients (IPST2011)* in Delft, the Netherlands, June 14-17, 2011
- [15] Q. Li, M. Wu, "Simulation method for the applications of ferromagnetic materials in suppressing high-frequency transients within GIS," *IEEE Trans. Power Delivery*, vol. 22, pp. 1628-1632, July 2007
- [16] W. D. Liu, L. J. Jin, J. L. Qian, "Simulation test of suppressing VFT in GIS by ferrite rings," in *Proc. 2001 International Symposium on Electrical Insulating Materials*, pp. 245-247, Beijing, China
- [17] J. V. G. Rama Rao, J. Amarnath, S. Kamakshaiha, "Simulation and measurement of Very Fast Transient Overvoltages in a 245 kV GIS and research on suppressing method using ferrite rings," *ARNP Journal of Engineering and Applied Sciences*, vol. 5, pp. 88-95, May 2010
- [18] S. Burow, S. Tenbohlen, W. Köhler, J. Smajic, A. Tröger, W. Holaus, "Can ferrite materials or resonant arrangements reduce the amplitudes of

- VFTO in GIS," in *Proc. 2011 17th International Symposium on High Voltage Engineering*, Hannover, Germany
- [19] S. Burow, U. Riechert, W. Köhler, S. Tenbohlen, "New mitigation methods for transient overvoltages in gas insulated substations," in *Proc. Stuttgarter Hochspannungssymposium*, Stuttgart, Germany, 2012, pp. 169-181
- [20] W. Piasecki, M. Fulczyk, M. Florkowski, P. Werle, O. Kouzmine, J. Szczechowski, "Mitigating VCB-induced very fast transients in industrial installations. Case study: arc furnace transformer," *CIGRE A2 & D1 2011*, Kyoto
- [21] Y. Guan, G. Yue, W. Chen, Z. Li, W. Liu, "Experimental Research on Suppressing VFTO in GIS by Magnetic Rings," *IEEE Trans. Power Delivery*, vol. 28, No. 4, pp. 2558-2565, Oct 2013
- [22] M. Golio, *The RF and Microwave Handbook*, CRC Press, 2001
- [23] COMSOL Multiphysics. [Online]. Available: www.comsol.com
- [24] D. J. Griffiths, "Introduction to Electrodynamics", 3rd edition, *Prentice Hall*, 1999
- [25] IEC 62271-102, "High-Voltage Switchgear and Controlgear – Part 102: Alternating Current Disconnectors and Earthing Switches"

VII. BIOGRAPHIES

Marcin Szweczyk (1974), Senior Member IEEE, received his M.Sc. and Ph.D. degree in Electrical Engineering from Warsaw University of Technology, Poland, in 2000 and 2009, respectively. Since February 2010 he has been with ABB Corporate Research in Cracow, Poland, as a researcher. His research and professional interests are mainly in the field of power system analyses and advanced simulations, transients analyses and transients mitigation, insulation coordination studies, 3D modelling and simulations of electromagnetic fields, and system concepts. He is also passionate about building highly effective teams in technology development area within complex world-wide learning organization. (ABB Corporate Research, Starowislna 13A, 31-038 Krakow, Poland, E-mail: marcin.szweczyk@pl.abb.com)



Wojciech Piasecki was born in Poland on May 15, 1966. He received the M.Sc. degree in electronics from the University of Science and Technology, in Kraków, Poland, and the Ph.D. degree from the Jagiellonian University, Kraków. He has been working for many years in electromagnetic and electrical phenomena, including high-frequency and nonlinear modeling of electrical equipment. Currently, he is a Researcher with the Corporate Research Center in Kraków. His main research concentrates around transient network phenomena analysis.



Marcin Wroński (1984), received M.Sc. degree in Physics from the AGH University of Science and Technology (UST) Kraków, Poland, in 2009. In the same year he started PhD studies parallel at the AGH UST and University Paris 13 in the co-tutelle system. He obtained double PhD degree in Physics and Mechanics of Materials, in 2013 (graduated with honors). He is currently working as a research assistant at AGH University of Science and Technology Kraków. His research interests are in the field of material science: development of polycrystalline deformation models, experimental work using EBSD and X-Ray diffraction technique. His research include modelling of electromagnetic fields using FEM.



Kamil Kutorasiński was born in 1985, received his M.Sc. in physics from the University of Science and Technology in Kraków, Poland where, from 2009, is the PhD student. His research are in the field of transport properties calculation in advanced material based on *ab initio* DFT methods as well as FEM modelling and simulations of electromagnetic fields. (Faculty of



Physics and Applied Computer Science, AGH University of Science and Technology, Al. A. Mickiewicza 30, 30-059 Krakow, Poland, E-mail: kamil.kutorasinski@fis.agh.edu.pl)